PTEP

Prog. Theor. Exp. Phys. **2022** 023D01(10 pages)
DOI: 10.1093/ptep/ptac004

Prediction of exotic hyperon halos in neutron-rich Zr hypernuclei

Ying Zhang[1,2,⋆], Hiroyuki Sagawa[2,3], and Emiko Hiyama[2,4]

[1]*Department of Physics, School of Science, Tianjin University, Tianjin, 300354, China.*
[2]*RIKEN Nishina Center, Wako, Saitama 351-0198, Japan*
[3]*Center for Mathematics and Physics, the University of Aizu, Aizu-Wakamatsu, Fukushima 965-8580, Japan*
[4]*Department of Physics, Tohoku University, 980-8578, Japan*
⋆E-mail: yzhangjcnp@tju.edu.cn

Received November 4, 2021; Revised January 5, 2022; Accepted January 10, 2022; Published January 12, 2022

We study the single- and double-Λ hypernuclei in Zr isotopes with the Hartree–Fock–Bogoliubov model and Skyrme-type nucleon–nucleon, Λ–nucleon, and Λ–Λ interactions. We found two peculiar features of the Λ hyperon halo phenomena that have never been found in nuclei without the strangeness degree of freedom. One is the *d*-wave halo, and the other is a bunch of three halo orbits just below the Λ hyperon threshold in ${}^{137}_{\Lambda}$Zr and also in ${}^{138}_{\Lambda\Lambda}$Zr. We name these exotic halo phenomena *giant hyperon halos* in hypernuclei whose core nucleus ^{136}Zr was predicted to have a "giant neutron halo." The interaction between Λ hyperons and the neutrons is responsible for inducing giant hyperon halo phenomena in the single- and double-Λ nuclei ${}^{137}_{\Lambda}$Zr and ${}^{138}_{\Lambda\Lambda}$Zr.

Subject Index D10, D14

1. Introduction

Since the first observation of a neutron halo in ^{11}Li [1], an unexpected phenomenon, the one- or two-nucleon halo structure has been intensively studied in neutron-/proton-rich nuclei from both experimental and theoretical sides [2–6]. Among these studies of halo structure, Ref. [6] predicted that up to six neutrons form the halo structure in neutron-rich Zr isotopes with neutron numbers larger than the magic number $N = 82$, which was called a "giant halo" structure [7,8]. In addition to most of the investigations being in the ground state, there are also discussions of halo structure in the excited states [9–12]. When one or two Λ hyperons are injected into such nuclei, due to the absence of the Pauli principle and the attraction between Λ and nucleon, the structure of the resultant Λ hypernuclei might be changed. Also, it is of interest to investigate the existence of exotic hyperon halos in single- and double-Λ hypernuclei stimulated by the giant halo structure of Zr isotopes.

There have been many theoretical studies of multi-strange hypernuclei [13–23]. In a recent article [24] we studied Λ hypernuclei in chains of carbon and boron isotopes in the Hartree–Fock (HF) model with Skyrme-type nucleon–nucleon (*NN*) and Λ–nucleon (Λ*N*) interactions, and we found the hyperon 1*p* state to be the halo orbit with an extended wave function far beyond the nuclear surface. Such Λ halo orbits have already been pointed out experimentally. For instance, the binding energy of hypertriton is 0.13 MeV with respect to the $d + \Lambda$ threshold; it is then expected to have a Λ halo structure in the ground state [25]. Moreover, the 1*p* state of

Λ in ${}^{13}_{\Lambda}$C has been observed to be 0.7 MeV [26] below the ^{12}C+Λ threshold, which is expected to have extended Λ density with respect to nucleon density in ^{12}C. The model is extended in this paper to apply to single-Λ and double-Λ hypernuclei in Zr isotopes. We will show that even more hyperon halo orbits exist in these heavy hypernuclei where the giant halo structure was predicted in the core nuclei.

For this calculation we adopt the Skyrme Hartree–Fock–Bogoliubov (HFB) model [27] to take into account the pairing correlations among nucleons, which is commonly used for the description of the gross properties of nuclei far from the stability line [28]. The original Skyrme HFB model has no strangeness degree of freedom. In this paper we extend this model to include one or two Λ hyperons.

2. Theoretical framework

For nucleons, the detailed HFB theory in the coordinate space for a finite nuclear system can be found in the literature [27]. We choose the SkI4 [29] parameter set for the NN interaction for the mean field and the density-dependent delta interaction (DDDI) for the pairing field, with which the giant neutron halo was predicted in Zr isotopes for $A > 122$ [6,7]. The pairing potential derived from the DDDI is

$$\Delta(r) = \frac{1}{2}V_0\left[1-\eta\left(\frac{\rho_N(r)}{\rho_0}\right)^{\alpha}\right]\tilde{\rho}_q(r), \qquad q = n, p, \tag{1}$$

where $\rho_N = \rho_n + \rho_p$ and $\tilde{\rho}_q$ are the local particle and pairing densities respectively. The parameters $V_0 = -300\,\text{MeV fm}^{-3}$, $\eta = 0.5$, $\alpha = 1.0$ and $\rho_0 = 0.16\,\text{fm}^{-3}$ were chosen as in Ref. [7]. The quasiparticle energy and total angular momentum cut-offs are $E_{\text{cut}} = 70\,\text{MeV}$ and $j = 15/2$ [7]. The HFB equation is solved by the mesh diagonalization method as in Ref. [30], with a box size of $R = 60$ fm and a mesh size of $\Delta r = 0.1$ fm. We use such a large box here since there are rather weakly bound Λ orbits, which will be shown later. This box size is much larger than the $R = 20$ fm used in Ref. [7]. However, with the same energy and angular momentum cut-offs, the neutron pairing gap obtained with $R = 60$ fm is 2% smaller than that obtained with $R = 20$ fm. Thus, the pairing properties are almost the same in both calculations.

The Skyrme-type ΛN interaction is taken as [31]

$$\begin{aligned} v_{\Lambda N}(\mathbf{r}_\Lambda - \mathbf{r}_N) = {} & t_0^\Lambda\left(1 + x_0^\Lambda P_\sigma\right)\delta(\mathbf{r}_\Lambda - \mathbf{r}_N) + \frac{1}{2}t_1^\Lambda[\boldsymbol{k}'^2\delta(\mathbf{r}_\Lambda - \mathbf{r}_N) + \delta(\mathbf{r}_\Lambda - \mathbf{r}_N)\boldsymbol{k}^2] \\ & + t_2^\Lambda \boldsymbol{k}'\delta(\mathbf{r}_\Lambda - \mathbf{r}_N)\cdot\boldsymbol{k} + iW_0^\Lambda \boldsymbol{k}'\delta(\mathbf{r}_\Lambda - \mathbf{r}_N)\cdot[(\boldsymbol{\sigma}_N + \boldsymbol{\sigma}_\Lambda)\times\boldsymbol{k}] \\ & + \frac{3}{8}t_3^\Lambda\left(1 + x_3^\Lambda P_\sigma\right)\delta(\mathbf{r}_\Lambda - \mathbf{r}_N)\rho^\gamma\left(\frac{\mathbf{r}_\Lambda + \mathbf{r}_N}{2}\right), \end{aligned} \tag{2}$$

where $\boldsymbol{k} = (\overrightarrow{\nabla}_\Lambda - \overrightarrow{\nabla}_N)/2i$ is the relative momentum operator acting on the wave functions on the right, $\boldsymbol{k}' = -(\overleftarrow{\nabla}_\Lambda - \overleftarrow{\nabla}_N)/2i$ acting on the left, and $P_\sigma = (1 + \boldsymbol{\sigma}_\Lambda\cdot\boldsymbol{\sigma}_N)/2$ is the spin-exchange operator. The resultant Hamiltonian density derived from the ΛN interaction $v_{\Lambda N}$ is [32]

$$\begin{aligned} \mathcal{H}_{\Lambda N} = {} & \frac{\hbar^2}{2m_\Lambda}\tau_\Lambda + t_0^\Lambda\left(1 + \frac{1}{2}x_0^\Lambda\right)\rho_\Lambda\rho_N + \frac{1}{4}\left(t_1^\Lambda + t_2^\Lambda\right)(\tau_\Lambda\rho_N + \tau_N\rho_\Lambda) \\ & + \frac{1}{8}\left(3t_1^\Lambda - t_2^\Lambda\right)\nabla\rho_\Lambda\cdot\nabla\rho_N + \frac{1}{2}W_0^\Lambda(\nabla\rho_N\cdot\boldsymbol{J}_\Lambda + \nabla\rho_\Lambda\cdot\boldsymbol{J}_N) \\ & + \frac{3}{8}t_3^\Lambda\left(1 + \frac{1}{2}x_3\right)\rho_N^{\gamma+1}\rho_\Lambda. \end{aligned} \tag{3}$$

In the above equation, ρ_B, τ_B, and $\boldsymbol{J}_B$ are the particle, kinetic energy, and spin densities respectively for baryons $B = N, \Lambda$, where $\rho_N = \rho_n + \rho_p$, $\tau_N = \tau_n + \tau_p$, and $\boldsymbol{J}_N = \boldsymbol{J}_n + \boldsymbol{J}_p$.

The interaction between the two Λ hyperons is also taken as Skyrme-type [14],

$$v_{\Lambda\Lambda}(\mathbf{r}_\Lambda - \mathbf{r}'_\Lambda) = \lambda_0\delta(\mathbf{r}_\Lambda - \mathbf{r}'_\Lambda) + \frac{1}{2}\lambda_1\left[\boldsymbol{k}'^2\delta(\mathbf{r}_\Lambda - \mathbf{r}'_\Lambda) + \delta(\mathbf{r}_\Lambda - \mathbf{r}'_\Lambda)\boldsymbol{k}^2\right] + \lambda_2\boldsymbol{k}'\delta(\mathbf{r}_\Lambda - \mathbf{r}'_\Lambda)\boldsymbol{k} + \lambda_3\delta(\mathbf{r}_\Lambda - \mathbf{r}'_\Lambda)\rho_N^\epsilon\left(\frac{\mathbf{r}_\Lambda + \mathbf{r}'_\Lambda}{2}\right). \tag{4}$$

The Hamiltonian density derived from the $\Lambda\Lambda$ interaction $v_{\Lambda\Lambda}$ is [14]

$$\mathcal{H}_{\Lambda\Lambda} = \frac{1}{4}\lambda_0\rho_\Lambda^2 + \frac{1}{8}(\lambda_1 + 3\lambda_2)\rho_\Lambda\tau_\Lambda + \frac{3}{32}(\lambda_2 - \lambda_1)\rho_\Lambda\nabla^2\rho_\Lambda + \frac{1}{4}\lambda_3\rho_\Lambda^2\rho_N^\epsilon. \tag{5}$$

For the two Λ hyperons we do not consider the pairing correlations between them, and thus describe them in the HF model. The terms in these Hamiltonian densities related to the nucleon densities ρ_N lead to the additional potentials in the nuclear mean field due to the addition of the Λ hyperons.

The single-Λ and double-Λ binding energies are defined as

$$B_\Lambda = B({}^{A+1}_{\Lambda}Z) - B({}^{A}Z), \tag{6}$$

$$B_{\Lambda\Lambda} = B({}^{A+2}_{\Lambda\Lambda}Z) - B({}^{A}Z), \tag{7}$$

where $B({}^{A+1}_{\Lambda}Z)$, $B({}^{A+2}_{\Lambda\Lambda}Z)$, and $B({}^{A}Z)$ are the total binding energies of the single-Λ hypernucleus, double-Λ hypernucleus, and normal nucleus respectively. The double-Λ gain energy is then defined as $\Delta B_{\Lambda\Lambda} = B_{\Lambda\Lambda} - 2B_\Lambda$.

In the calculation, the Skyrme-type ΛN interaction is taken from parameter set No. 5 in Ref. [31] obtained by the G-matrix calculation from the one-boson-exchange potential. In particular, this interaction includes the ΛN spin–orbit interaction with the original strength $W_0^\Lambda = 62\,\text{MeV fm}^5$. However, we found that the obtained spin–orbit splitting of the $1p$ states in ${}^{13}_{\Lambda}$C is too large compared to the experimental data of 0.152 MeV [33]. Therefore, we use a reduced value of $W_0^\Lambda = 4.4\,\text{MeV fm}^5$ (labeled "LY5r") instead, and obtain the spin–orbit splitting 0.153 MeV for the $1p$ states in ${}^{13}_{\Lambda}$C calculated together with the NN interaction SkI4.

The $\Lambda\Lambda$ interaction is chosen as "S$\Lambda\Lambda$1" as proposed in Ref. [14], with $\lambda_1 = 57.5\,\text{MeV fm}^5$, $\lambda_2 = 0$, and $\lambda_3 = 0$. The original value of $\lambda_0 = -312.6\,\text{MeV fm}^3$ is tuned to be $\lambda_0 = -50.0\,\text{MeV fm}^3$ (labeled "S$\Lambda\Lambda$1r") according to the experimental data from the NAGARA event [34,35]. Together with the NN interaction SkI4 and the above tuned ΛN, $\Lambda\Lambda$ interactions, the calculated single-Λ binding energy in ${}^{5}_{\Lambda}$He is $B_\Lambda^{\text{cal.}} = 3.51$ MeV, the double-Λ binding energy in ${}^{6}_{\Lambda\Lambda}$He is $B_{\Lambda\Lambda}^{\text{cal.}} = 7.56$ MeV, and the double-Λ gain energy is $\Delta B_{\Lambda\Lambda}^{\text{cal.}} = 0.54$ MeV. These are consistent with the experimental data $B_\Lambda^{\text{expt.}} = 3.12 \pm 0.02$ MeV [36], $B_{\Lambda\Lambda}^{\text{expt.}} = 6.91 \pm 0.16$ MeV [35], and $\Delta B_{\Lambda\Lambda}^{\text{expt.}} = 0.67 \pm 0.17$ MeV [35] respectively.

Using the NN interaction SkI4, ΛN interaction LY5r, and $\Lambda\Lambda$ interaction S$\Lambda\Lambda$1r, the calculated double-Λ binding energy $B_{\Lambda\Lambda}^{\text{cal.}}$ and the gain energy $\Delta B_{\Lambda\Lambda}^{\text{cal.}}$ of several light double-Λ hypernuclei are listed in Table 1, together with the experimental data [35,37].

3. Results and discussion

First, we list the calculated bulk properties of single- and double-Λ hypernuclei for ^{90,114,136}Zr isotopes in Table 2, including the rms radius of neutron, proton, and Λ hyperon; the average neutron and proton pairing gaps; the single- or double-Λ binding energies; and the double-Λ

Table 1. The calculated double-Λ binding energy $B^{\rm cal.}_{\Lambda\Lambda}$ and the gain energy $\Delta B^{\rm cal.}_{\Lambda\Lambda}$ for several light double-Λ hypernuclei together with the experimental data [35,37]. All the energies are in MeV.

Nuclide	$B^{\rm cal.}_{\Lambda\Lambda}$	$B^{\rm expt.}_{\Lambda\Lambda}$	$\Delta B^{\rm cal.}_{\Lambda\Lambda}$	$\Delta B^{\rm expt.}_{\Lambda\Lambda}$
${}^{6}_{\Lambda\Lambda}$He	7.564	6.91 ± 0.16 (NAGARA)	0.536	0.67 ± 0.17
${}^{11}_{\Lambda\Lambda}$Be	18.594	20.86 ± 3.06 (MIKAGE)	0.478	2.64 ± 3.09
		22.12 ± 2.67 (MIKAGE)		3.90 ± 2.71
		20.83 ± 1.27 (HIDA)		2.61 ± 1.34
		19.07 ± 0.11 (MINO)		1.87 ± 0.37
${}^{13}_{\Lambda\Lambda}$B	22.221	23.3 ± 0.7 (KEK-E176)	0.435	0.6 ± 0.8

Table 2. Bulk properties of Zr isotopes with one or two Λ hyperons: rms radius $r^{n}_{\rm rms}$, $r^{p}_{\rm rms}$, $r^{\Lambda}_{\rm rms}$ (fm), the average pairing gap Δ_n, Δ_p (MeV), single- or double-Λ binding energies $B_{\Lambda(\Lambda)}$ (MeV), and double-Λ gain energy $\Delta B_{\Lambda\Lambda}$ (MeV). The Λ hyperon(s) is (are) placed in the ground state $1s_{1/2}$ orbit.

	$r^{n}_{\rm rms}$	$r^{p}_{\rm rms}$	$r^{\Lambda}_{\rm rms}$	Δ_n	Δ_p	$B_{\Lambda(\Lambda)}$	$\Delta B_{\Lambda\Lambda}$
^{90}Zr	4.2674	4.1588		0.000	0.915		
${}^{91}_{\Lambda}$Zr	4.2608	4.1515	3.1346	0.000	0.901	23.468	
${}^{92}_{\Lambda\Lambda}$Zr	4.2543	4.1445	3.1197	0.000	0.889	47.123	0.188
^{114}Zr	4.8000	4.4112		0.953	0.796		
${}^{115}_{\Lambda}$Zr	4.7934	4.4036	3.3059	0.953	0.785	23.868	
${}^{116}_{\Lambda\Lambda}$Zr	4.7870	4.3962	3.2897	0.952	0.773	47.905	0.169
^{136}Zr	5.4649	4.5415		0.620	0.602		
${}^{137}_{\Lambda}$Zr	5.4585	4.5328	3.4003	0.593	0.579	24.074	
${}^{138}_{\Lambda\Lambda}$Zr	5.4520	4.5244	3.3823	0.568	0.556	48.315	0.168

gain energies. The average pairing gap for neutron and proton is defined as

$$\Delta_q = \frac{\int d\mathbf{r}\Delta(\mathbf{r})\tilde{\rho}_q(\mathbf{r})}{\int d\mathbf{r}\tilde{\rho}_q(\mathbf{r})}, \qquad q = n, p. \tag{8}$$

Here, the Λ hyperon(s) is (are) placed in the lowest $1s_{1/2}$ orbit. One finds fast growth of the neutron rms radius as the neutron number increases compared to the proton and Λ hyperon radii. For Zr isotopes, adding one and two Λ hyperons, both the neutron and proton rms radii shrink slightly due to the "glue-like" role of the Λ hyperon. The addition of the Λ hyperon could also reduce the pairing gaps, which is more obvious in ^{136}Zr. The single- or double-Λ binding energies and the double-Λ gain energies are almost the same among these three Zr hypernuclei. It is natural to see that the double-Λ binding energies of these three Zr hypernuclei are much larger than those of the light hypernuclei, as shown in Table 1. However, the double-Λ gain energy is only 30% of that in the lighter hypernucleus ${}^{6}_{\Lambda\Lambda}$He. This suggests that the ΛΛ interaction could be suppressed by a larger extension of the Λ wave function in heavier isotopes, and by the short-range character of this interaction, as predicted in Refs. [38–40].

Three neutron mean-field potentials and the single-particle levels of ${}^{91}_{\Lambda}$Zr, ${}^{115}_{\Lambda}$Zr, and ${}^{137}_{\Lambda}$Zr are shown in Fig. 1. The depths of the three potentials are essentially the same at around −70 MeV, while the width and the surface diffuseness become wider for the heavier Zr hypernuclei. Consequently, most of the single-neutron levels shift down, and rather weakly bound $3p$ orbits appear in ${}^{137}_{\Lambda}$Zr just below the neutron threshold. Actually, as a remarkable feature of the core nucleus

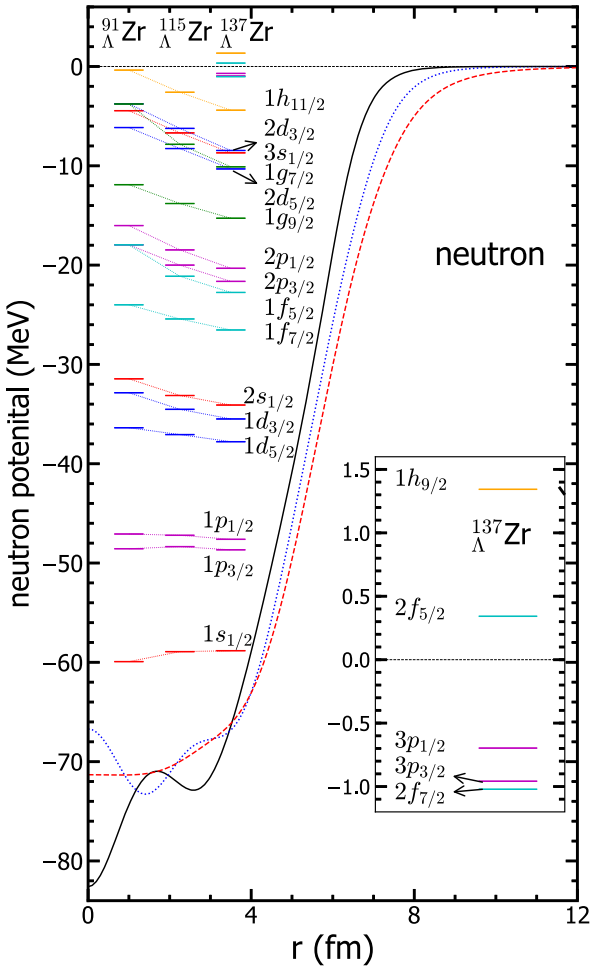

Fig. 1. The neutron single-particle energies and potentials in the hypernuclei $^{91}_{\Lambda}$Zr (solid line), $^{115}_{\Lambda}$Zr (dotted line), and $^{137}_{\Lambda}$Zr (dashed line) calculated with a Λ hyperon in the $1s_{1/2}$ state. The states within $-1.0 \sim 1.5$ MeV in $^{137}_{\Lambda}$Zr are enlarged in the inset.

^{136}Zr, it was found in Ref. [6] that the neutron single-particle states $3p_{3/2}$ and $3p_{1/2}$ are bound less than 1 MeV below the neutron threshold, and up to six neutrons in the two p orbits create the so-called *giant halo* due to their extended wave functions. This giant halo phenomenon is induced by an extended surface diffuseness of the potential beyond $r = 8$ fm, as can be clearly seen in Fig. 1.

The Λ mean-field potentials and the single-particle levels of the three Zr hypernuclei are shown in Fig. 2. Because of the strong ΛN interaction, each Λ single-particle potential has similar characteristic features to the neutron single-particle potential of the corresponding core nucleus as far as the surface diffuseness is concerned. It should also be noticed that the depths of the three potentials are the same at around -30 MeV, while the surface part is very much changed. Similar to the neutron mean-field potential, the width and the surface diffuseness are larger for the heavier Zr hypernuclei. It is a surprise to find that the hyperon $3s_{1/2}$, $2d_{5/2}$, and $2d_{3/2}$ states are almost degenerate just below the Λ threshold in $^{137}_{\Lambda}$Zr.

Assuming there is one Λ hyperon in the excited $3s_{1/2}$ state, the single-Λ wave functions of the $3s_{1/2}$, $2d_{3/2}$ and $1g_{7/2}$ orbits are shown in Fig. 3(a). They can create very extended Λ halo wave functions, as shown in Fig. 3(a), and produce the rms radii $r^{\Lambda}_{\rm rms} \approx 10$ fm for the $3s_{1/2}$ state and

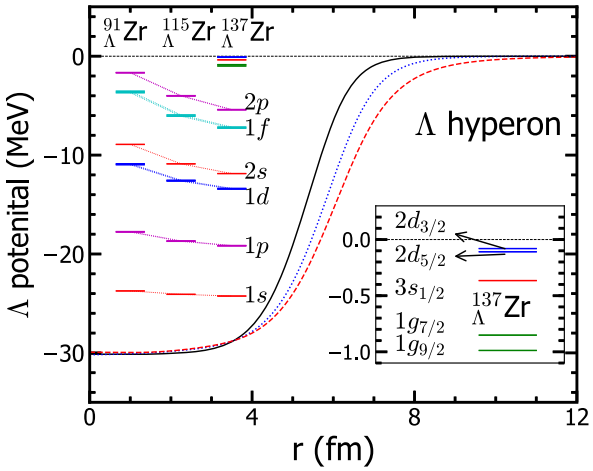

Fig. 2. The Λ single-particle energies and potentials in the hypernuclei $^{91}_{\Lambda}$Zr (solid line), $^{115}_{\Lambda}$Zr (dotted line), and $^{137}_{\Lambda}$Zr (dashed line) calculated with a Λ hyperon in the $1s_{1/2}$ state. The states within $-1.0 \sim 0$ MeV in $^{137}_{\Lambda}$Zr are enlarged in the inset.

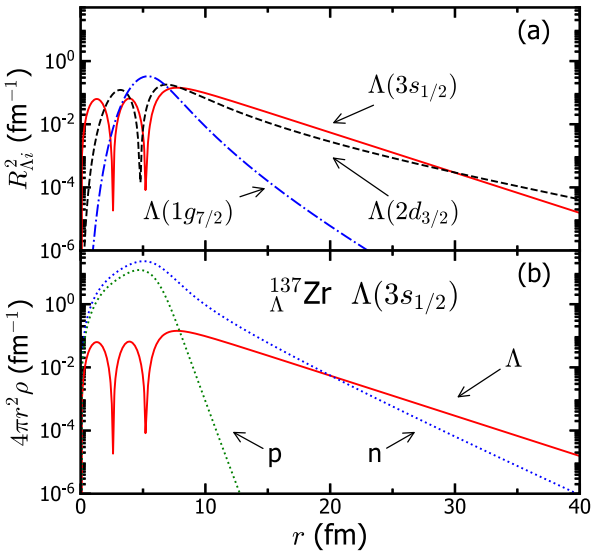

Fig. 3. (a) Λ single-particle wave functions $R^2_{\Lambda i}$ for the $3s_{1/2}$, $2d_{3/2}$, and $1g_{7/2}$ states. (b) Neutron, proton, and Λ hyperon densities $4\pi r^2\rho$ in $^{137}_{\Lambda}$Zr, where the Λ hyperon is in the $3s_{1/2}$ state.

$r^{\Lambda}_{\rm rms} \approx 8.5$ fm for the $2d$ states, as shown in Table 3. These rms radii are close to or even larger than that of the neutron halo $3p$ states in the core nucleus ^{136}Zr. As a result, the Λ hyperon in the excited $3s_{1/2}$ state can produce a much longer tail of the density compared to the giant neutron halo density of the core nucleus ^{136}Zr in Fig. 3(b). We name this bunching of hyperon halo orbits the *giant hyperon halo* phenomenon in the neutron-rich hypernucleus $^{137}_{\Lambda}$Zr. The physical meaning of the term "giant hyperon halo" is twofold. First, the rms radii $r^{\Lambda}_{\rm rms}$ of these Λ hyperon states are almost twice as large as the radius of the core nucleus, even larger than that of the neutron halo orbits. Second, the bunch of three halo orbits $3s$ and $2d$ can accommodate from one to 12 Λ hyperons at the maximum, which would be more than the halo neutrons in the core nucleus, forming a giant neutron halo. However, we would like to add a note of caution,

Table 3. Single-particle energy (s.p.e.) in MeV, the occupation probability v^2, and the rms radius $r_{\rm rms}$ (fm) of the single-particle level of neutron and Λ in ${}^{137}_{\Lambda}$Zr. The Λ is in the $3s_{1/2}$ orbit. The results for the neutron are calculated with the corresponding canonical states, and those of Λ are calculated with the HF single-particle states.

	State	s.p.e.	v^2	$r_{\rm rms}$
n	$3p_{1/2}$	− 0.726	0.872	8.7611
	$3p_{3/2}$	− 0.986	0.926	8.3981
	$2f_{5/2}$	0.292	0.155	7.2496
	$2f_{7/2}$	− 1.047	0.886	6.9517
	$1h_{9/2}$	1.271	0.050	6.1079
	$1h_{11/2}$	− 4.432	0.992	5.7730
Total				5.4624
Λ	$3s_{1/2}$	− 0.370	0.500	9.9822
	$2d_{3/2}$	− 0.090	0.0	8.5794
	$2d_{5/2}$	− 0.118	0.0	8.4148
	$1g_{7/2}$	− 0.870	0.0	5.8904
	$1g_{9/2}$	− 1.006	0.0	5.8721

in that these single- or multi-hyperon states are excited states and need serious efforts to create them experimentally in the future. Furthermore, these states could also be dependent on the ΛΛ interaction while more and more hyperons are added inside the nucleus. However, there is still a large ambiguity of the ΛΛ interaction due to the lack of data. It should be noted that these "giant hyperon halo" states are predicted by using the present ΛΛ interaction of Eq. (5) determined by the available data.

In normal nuclei, nucleons in the low-angular-momentum single-particle states $\ell \leq 1$, namely only *s*- and *p*-orbit nucleons, can create the halo phenomenon when the single-particle energy becomes very close to the particle threshold [41,42], typically less than 1 MeV. However, in the case of neutron-rich hypernuclei, the Λ hyperon in the *d*-orbit can also show the nature of the halo wave function. Comparing with the neutron mean-field potential and single-particle levels in Fig. 1, this unique feature of the Λ hyperon may be created by the shallow Λ potential, less than half of the nuclear potential, and the largely extended surface diffuseness shown in Fig. 2. Then, the 2*d* states are captured in this extended pocket of the potential and show a halo character, which never appears in normal nuclei without the strangeness degree of freedom. Also, due to the small spin–orbit splitting suggested by the experimental data for ${}^{13}_{\Lambda}$C, the two 2*d* orbits are nearly degenerate just below the threshold. Thus, as stated before, the bunch of three halo orbits 3*s* and 2*d* can hold from one to 12 Λ hyperons at the maximum to form the "giant hyperon halo" phenomenon. Indeed, such a halo structure in the excited state should have a very short life and be difficult to measure, and it could be very difficult to produce such a neutron-rich hypernucleus with so many hyperons at present; it is still interesting to predict such halo orbits for future theoretical and experimental investigations.

We would also like to discuss whether the bunch of three almost degenerate weakly bound states 3*s* and 2*d* just below the hyperon threshold in the double-Λ hypernucleus ${}^{138}_{\Lambda\Lambda}$Zr is related to the Efimov effect. It is known that the Efimov states appear as a bunch of loosely-bound states just below the threshold energy induced by an attractive correlation on the particles in the continuum. They are also called "Borromean states" similar to the "Borromean" nucleus

^{11}Li. In multi-hyperon nuclei, the hyperon–hyperon interaction will play a role of creating the hyperon Efimov states. So far, experimental information for the $\Lambda\Lambda$ interaction is known only in a few *p*-shell nuclei. The double-Λ gain energies are observed to be rather small. We fix the present $\Lambda\Lambda$ interaction to reproduce the observed double-Λ binding energy $B_{\Lambda\Lambda}$ and the double-Λ gain energy $\Delta B_{\Lambda\Lambda}$ of ${}^{6}_{\Lambda\Lambda}$He. Using this $\Lambda\Lambda$ interaction, the calculated results together with the experimental data for ${}^{6}_{\Lambda\Lambda}$He, ${}^{11}_{\Lambda\Lambda}$Be, and ${}^{13}_{\Lambda\Lambda}$B are tabulated in Table 1. We found that the calculated double-Λ gain energies $\Delta B_{\Lambda\Lambda}$ are all rather small, $\sim$0.5 MeV, in these three double-Λ nuclei. As a result, the calculated Λ single-particle potentials of the three double-Λ Zr hypernuclei are essentially the same as those of the corresponding single-Λ Zr hypernuclei. Then, the Λ hyperon states $3s_{1/2}$, $2d_{5/2}$, and $2d_{3/2}$ are almost unchanged, and no more weakly bound states appear when adding one more Λ hyperon inside ${}^{137}_{\Lambda}$Zr. Therefore, the bunch of three almost degenerate states $3s$ and $2d$ are not related to the Efimov effect here. However, as seen in Table 1, although with a large uncertainty, the experimental double-Λ gain energy $\Delta B_{\Lambda\Lambda}$ in ${}^{11}_{\Lambda\Lambda}$Be is several times larger than the present model prediction. If this is the case, we need a much stronger $\Lambda\Lambda$ interaction to reproduce the data. This interaction may pull more continuum states close to the Λ threshold down to be degenerate weakly bound orbits, due to adding one more Λ hyperon inside ${}^{137}_{\Lambda}$Zr. Therefore, we need more precise experimental data for double-Λ hypernuclei, especially in the larger-mass region, to confirm the possible Efimov effect in double-Λ hypernuclei.

Actually, the giant hyperon halo orbits $3s$ and $2d$ found in ${}^{137}_{\Lambda}$Zr could also be dependent on the ΛN and $\Lambda\Lambda$ interactions. It is noted that, in the present ΛN interaction LY5r, the spin–orbit strength is reduced compared to its original value in LY5 to reproduce the data for the spin–orbit splitting in ${}^{13}_{\Lambda}$C. The $\Lambda\Lambda$ interaction S$\Lambda\Lambda$1r has a reduced strength λ_0 compared to its original value in S$\Lambda\Lambda$1 to reproduce the binding energy of ${}^{6}_{\Lambda\Lambda}$He. It is interesting to check whether these giant hyperon halo orbits found in ${}^{137}_{\Lambda}$Zr are there or not when we use the original ΛN and $\Lambda\Lambda$ interactions LY5 and S$\Lambda\Lambda$1. Figure 4(a) shows the Λ single-particle energies in the hypernucleus ${}^{137}_{\Lambda}$Zr calculated with LY5 and LY5r, where the Λ hyperon is in the ground state $1s_{1/2}$. The corresponding Λ single-particle potentials calculated with LY5 and LY5r are shown by solid and dashed lines respectively, and are almost the same. The inset zooms in on the weakly bound levels near the threshold. One can still find the $3s_{1/2}$ and $2d_{5/2}$ orbits to be weakly bound calculated with LY5. Due to the large spin–orbit potential strength in LY5, the $2d_{3/2}$ orbit is not bound. Figure 4(b) and the inset show the Λ single-particle energies in the hypernucleus ${}^{138}_{\Lambda\Lambda}$Zr calculated with LY5 + S$\Lambda\Lambda$1 and LY5r + S$\Lambda\Lambda$1r, where the two Λ hyperons are both in the ground state $1s_{1/2}$. Due to the large strength of λ_0 in S$\Lambda\Lambda$1, the $2d_{3/2}$ level is pulled down to be weakly bound. As a result, both LY5 + S$\Lambda\Lambda$1 and LY5r + S$\Lambda\Lambda$1r can produce the giant Λ halo orbits $3s$ and $2d$ in ${}^{138}_{\Lambda\Lambda}$Zr. The solid Λ single-particle potential line is the result calculated by LY5 + S$\Lambda\Lambda$1, which is deeper at the bottom than the dashed line calculated by LY5r + S$\Lambda\Lambda$1r because of the more attractive $\Lambda\Lambda$ interaction. However, their diffusive behaviors around the hypernucleus surface are common, which are decisive in holding those weakly bound $3s$ and $2d$ orbits.

4. Summary

We investigated the Λ hyperon states in the single-Λ and double-Λ Zr hypernuclei with the Skyrme HFB model. The ΛN and $\Lambda\Lambda$ interactions are adjusted according to the available

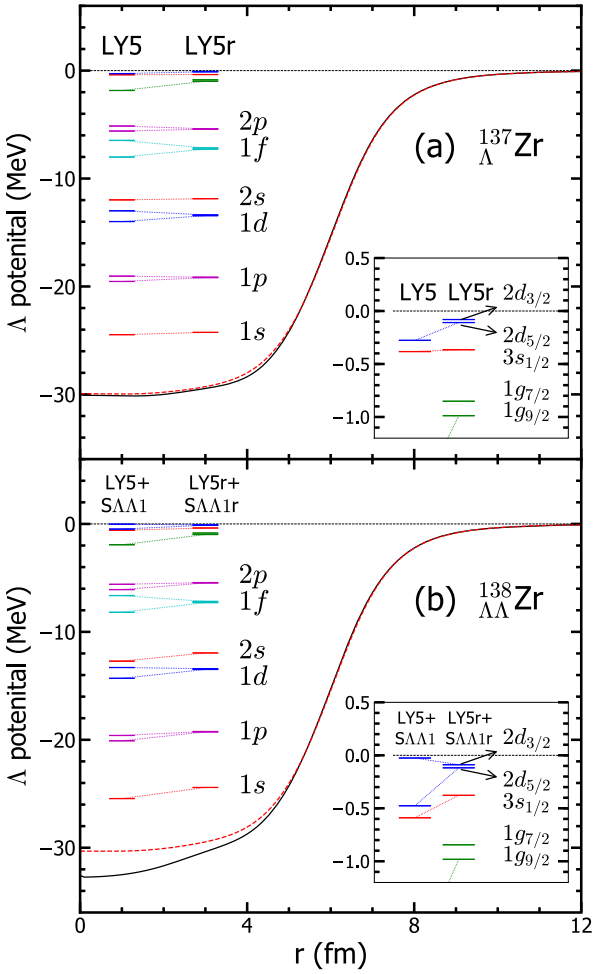

Fig. 4. The Λ single-particle energies and potentials in the hypernuclei (a) $^{137}_{\Lambda}$Zr and (b) $^{138}_{\Lambda\Lambda}$Zr. In panel (a), the single-particle energies are obtained by using the Λ*N* interactions LY5 and LY5r; the corresponding Λ single-particle potentials are denoted by the solid and dashed lines respectively. In panel (b), the results are obtained by using the Λ*N* and ΛΛ interactions LY5 + SΛΛ1 and LY5r + SΛΛ1r; the corresponding Λ single-particle potentials are denoted by the solid and dashed lines respectively. The Λ hyperon(s) is (are) in the ground state $1s_{1/2}$. The states within $-1.0 \sim 0$ MeV are enlarged in the insets.

experimental data for light single- and double-Λ hypernuclei. It is interesting to find that the double-Λ gain energy in the Zr hypernucleus is only 30% of those in the light hypernuclei. This may suggest that the ΛΛ interaction could be suppressed by the interactions between the Λ and more nucleons. In particular, adding one or two Λ hyperons inside the neutron-rich nucleus ^{136}Zr, which was predicted to have a giant neutron halo, we found the very weakly bound and almost degenerate 3*s* and 2*d* orbits for the Λ hyperon. These states appear because of the diffusive Λ single-particle potential determined by the extended neutron densities. We name them "giant hyperon halo" orbits, since their rms radii are even larger than those of the neutron halo orbits 3*p*, and these three weakly bound orbits can hold even more Λ hyperons than the neutrons in the giant neutron halo structure.

Acknowledgments

This work was supported by JSPS KAKENHI Grant Numbers JP19K03858, JP18H05407, and 20H00155, and by the China Scholarship Council (Grant No. 201906255002).

References

[1] I. Tanihata, H. Hamagaki, O. Hashimoto, Y. Shida, N. Yoshikawa, K. Sugimoto, O. Yamakawa, T. Kobayashi, and N. Takahashi, Phys. Rev. Lett. **55**, 2676 (1985).
[2] A. S. Jensen, K. Riisager, D. V. Fedorov, and E. Garrido, Rev. Mod. Phys. **76**, 215 (2004).
[3] B. Jonson, Phys. Rep. **389**, 1 (2004).
[4] K. Hagino, I. Tanihata, and H. Sagawa, Exotic nuclei far from the stability line, in *100 Years of Subatomic Physics*, eds. E. M. Henley Henley and S. D. Ellis Ellis (World Scientific, Singapore, 2013), p. 231.
[5] J. Meng and S. G. Zhou, J. Phys. G **42**, 093101 (2015).
[6] J. Meng and P. Ring, Phys. Rev. Lett. **80**, 460 (1998).
[7] M. Grasso, S. Yoshida, N. Sandulescu, and N. Van Giai, Phys. Rev. C **74**, 064317 (2006).
[8] Y. Zhang, M. Matsuo, and J. Meng, Phys. Rev. C **86**, 054318 (2012).
[9] K. Riisager, Phys. Scr. T **152**, 014001 (2013).
[10] J. Al-Khalili and K. Arai, Phys. Rev. C **74**, 034312 (2006).
[11] C. Romero-Redondo, E. Garrido, D. V. Fedorov, and A. S. Jensen, Phys. Lett. B **660**, 32 (2008).
[12] M. Yu, P.-F. Zhang, T.-N. Ruan, and J.-Y. Guo, Mod. Phys. Lett. A **21**, 2751 (2006).
[13] M. Rufa, J. Schaffner, J. Maruhn, H. Stöcker, W. Greiner, and P.-G. Reinhard, Phys. Rev. C **42**, 2469 (1990).
[14] D. E. Lanskoy, Phys. Rev. C **58**, 3351 (1998).
[15] E. Hiyama, M. Kamimura, T. Motoba, T. Yamada, and Y. Yamamoto, Phys. Rev. C **66**, 024007 (2002).
[16] H. F. Lv and J. Meng, Chinese Phys. Lett. **19**, 1775 (2002).
[17] H. F. Lv, Chinese Phys. Lett. **25**, 3613 (2008).
[18] A. Gal and D. J. Millener, Phys. Lett. B **701**, 342 (2011).
[19] H. J. Schulze and T. Rijken, Phys. Rev. C **88**, 024322 (2013).
[20] E. Khan, J. Margueron, F. Gulminelli, and A. R. Raduta, Phys. Rev. C **92**, 044313 (2015).
[21] H. Güven, K. Bozkurt, E. Khan, and J. Margueron, Phys. Rev. C **98**, 014318 (2018).
[22] Y. Tanimura, Phys. Rev. C **99**, 034324 (2019).
[23] Y. T. Rong, P. Zhao, and S. G. Zhou, Phys. Lett. B **807**, 135533 (2020).
[24] Y. Zhang, H. Sagawa, and E. Hiyama, Phys. Rev. C **103**, 034321 (2021).
[25] K. Miyagawa, H. Kamada, W. Glöckle, H. Yamamura, T. Mart, and C. Bennhold, Proc. 1st Asian-Pacific Conf. on Few-Body Problems in Physics, p. 324 (2000).
[26] M. May et al., Phys. Rev. Lett. **78**, 4343 (1997).
[27] J. Dobaczewski, H. Flocard, and J. Treiner, Nucl. Phys. A **422**, 103 (1984).
[28] M. Bender, P.-H. Heenen, and P.-G. Reinhard, Rev. Mod. Phys. **75**, 121 (2003).
[29] P.-G. Reinhard and H. Flocard, Nucl. Phys. A **584**, 467 (1995).
[30] Y. Zhang, M. Matsuo, and J. Meng, Phys. Rev. C **90**, 034313 (2014).
[31] D. E. Lanskoy and Y. Yamamoto, Phys. Rev. C **55**, 2330 (1997).
[32] N. Guleria, S. K. Dhiman, and R. Shyam, Nucl. Phys. A **886**, 71 (2012).
[33] S. Ajimura et al., Phys. Rev. Lett. **86**, 4255 (2001).
[34] H. Takahashi et al., Phys. Rev. Lett. **87**, 212502 (2001).
[35] K. Nakazawa and H. Takahashi, Prog. Theor. Phys. Suppl. **185**, 335 (2010).
[36] D. H. Davis, Nucl. Phys. A **754**, 3 (2005).
[37] H. Ekawa et al., Prog. Theor. Exp. Phys. **2019**, 021D02 (2019).
[38] D. E. Lanskoy, Y. A. Lurie, and A. M. Shirokov, Z. Phys. A **357**, 95 (1997).
[39] S. Marcos, R. J. Lombard, and J. Mareš, Phys. Rev. C **57**, 1178 (1998).
[40] J. Caro, C. García-Recio, and J. Nieves, Nucl. Phys. A **646**, 299 (1999).
[41] H. Sagawa, Phys. Lett. B **286**, 7 (1992).
[42] K. Riisager, A. S. Jensen, and P. Möller, Nucl. Phys. A **548**, 393 (1992).